DOI: 10.1002/ejic.200500829

Binding of an Oxo-Bridged Dinuclear Iron(III) Complex $\{[Fe(phen)(H_2O)_3]_2O\}(SO_4)_2$ to DNA and Its Recognition of Single- and Double-Stranded DNA As Determined by Electrochemical Studies

Qing Xiang Wang,[a] Kui Jiao,*[a] Wei Sun,[a] Fang Fang Jian,[b] and Xuan Hu[a]

Keywords: Oxo-bridged diiron(III) complex / Crystallography / DNA recognition / Voltammetry

An oxo-bridged dinuclear iron(III) complex, $\{[Fe(phen)(H_2O)_3]_2O\}(SO_4)_2$, was synthesized and the molecular structure was determined by X-ray crystallography. Cyclic voltammetry shows that the complex has a cathodic peak at +0.325 V and a pair of redox peaks at +1.011 V and +0.811 V, respectively, which can be explained by an EC–C–EC mechanism. The binding property of the complex to fish-sperm DNA was investigated by electronic absorption spectrophotometry and electrochemical methods. The change in the electrochemical behavior of the complex after treatment with DNA shows that the oxo-bridged diiron(III) complex interacts with DNA mainly through electrostatic binding, while the electrochemical and chemical (EC–C) process product interacts mainly by intercalation. This result is further supported by experiments examining the influence of ionic strength. The difference in the binding modes of $\{[Fe(phen)(H_2O)_3]_2O\}(SO_4)_2$ and its EC–C product, namely a mononuclear phen-ligated ferrous complex, to DNA implies that this strategy can be used to distinguish single-stranded (ss-) and double-stranded (ds-) DNA.
(© Wiley-VCH Verlag GmbH & Co. KGaA, 69451 Weinheim, Germany, 2006)

Introduction

Studies on the interaction between DNA and small molecules are central to probing the accurate local structures of DNA,[1–5] and to understanding the natural DNA-mediated biological mechanisms.[6] The fields of applied pharmacology, novel drug design[7–8] and chemotherapy[9] also emphasize the interactions of small molecules with DNA. Among DNA-binding molecules, iron complexes with the ligands 1,10-phenanthroline (phen) or modified phen are particularly attractive because these metal complexes can effectively bind to DNA through different modes[10–13] and the iron ions and the ligands of these complexes can easily be controlled to facilitate the clear study of the DNA-binding mechanism.[14–15]

A number of studies have addressed the synthesis of a series of mononuclear iron-phen complexes and their interaction with DNA.[16–20] However, compared with the mononuclear iron complexes, the synthesis and interaction with DNA of dinuclear iron complexes have received much less attention.[21–24] Que Jr. et al.[22] have reported a dinuclear ferric complex, $Fe_2(HPTB)(OH)(NO_3)_4$ [HPTB = *N*,*N*,*N*′,*N*′′-tetrakis(2-benzimidazolylmethyl)-2-hydroxy-1,3-diaminopropane], and found that, in the presence of hydrogen peroxide or O_2 and a reductant, this diiron complex can promote the cleavage of plasmid DNA in a "hydrolytic fashion". This is similar to the DNA cleavage mediated by the Fe–bleomycin complex and its mimetic compounds.[23] Additionally, Xu et al.[24] have investigated the interaction of DNA with a diiron complex $Fe_2(DTPB)(\mu\text{-}O)(\mu\text{-}Ac)Cl(BF_4)_2$ [DTPB = 1,1,4,7,7-penta(2′-benzimidazol-2-ylmethyl)triazaheptane, Ac = acetate] by spectroscopic methods. In addition, the hydrolytic cleavage of the supercoiled and linear DNA by the diiron complex was supported by evidence from anaerobic reactions, free-radical quenching, high-performance liquid chromatography experiments, enzymatic manipulation, footprinting analysis, and so forth.

On the other hand, nonheme oxo-bridged dinuclear iron(III) complexes have been extensively studied because of their distinctive magnetic and spectroscopic properties.[25–26] Furthermore, the significant biological activity of these kinds of dinuclear complexes has also attracted considerable attention from researchers, as they can provide structural models for diiron sites in nonheme proteins, such as ribonucleotide reductase, which converts ribonucleotides into deoxyribonucleotides in the first step in the biosynthesis of DNA.[27–29] However, only a few crystal structures of dinuclear iron(III) complexes with phenanthroline as a terminal ligand have been reported to date.[30] Knowledge of the exact molecular structure, and electrochemical and DNA-binding properties of nonheme oxo-bridged dinuclear

[a] College of Chemistry and Molecular Engineering, Qingdao University of Science and Technology,
Qingdao, 266042 P. R. China
Fax: +86-532-84855916
E-mail: kjiao@qust.edu.cn
[b] The Laboratory of New Materials and Functional Compounds, Qingdao University of Science and Technology,
Qingdao, 266042 P. R. China.

 InterScience © 2006 Wiley-VCH Verlag GmbH & Co. KGaA, Weinheim

iron(III) complexes will be helpful for us to understand the reaction mechanisms of these active models in cells and the body.

Herein we report the synthesis, crystal structure, and electrochemical property of a new oxo-bridged dinuclear iron(III) complex with the ligand phen, $\{[Fe(phen)(H_2O)_3]_2O\}(SO_4)_2$. Additionally, we paid particular attention to the binding properties of this dinuclear iron(III) complex to DNA by using absorption spectroscopic and voltammetric methods. The notable phenomenon is that the dinuclear iron complex, and its EC–C mononuclear product (EC and C mean electrochemical process and chemical dissociation process, respectively), bind to DNA through different modes under the same conditions. This suggests that, on the basis of its electrochemical behavior, the complex could be an effective recognition probe for dsDNA and ssDNA. We also hope that this investigation is of value for the understanding of the biological mechanism in nonheme protein–DNA interactions and of the structure–activity relationship of nonheme oxo-bridged dinuclear iron(III) complexes in biological processes.

Results and Discussion

Crystal Structure of the Title Oxo-Bridged Diiron(III) Compound

The crystal structure of the title compound consists of discrete molecules in which all the atoms lie on general positions. The molecular structure of the complex is illustrated in Figure 1. The cationic complex of $\{[Fe(phen)(H_2O)_3]_2O\}^{4+}$ has a C_2 symmetry axis through the bridging O(6) atom. The two sulfate anions are present in the lattice to balance the charge. The iron atoms are surrounded by two nitrogen and four oxygen atoms to form a distorted octahedral geometry. The two parts of the dinuclear iron(III) cation complex are bridged by the O(6) atom. Three water molecues coordinate to the Fe^{III} ion, with Fe–O distances of 2.004(4) Å, 2.019(4) Å, and 2.153(4) Å for Fe(1)–O(5), Fe(1)–O(7), and Fe(1)–O(8), respectively. The Fe–O–Fe linkage is nonlinear, exhibiting an angle of 163.9(4)° for Fe(1)–O(6)–Fe(1A). The Fe–μ-O(6) distance [1.7877(12) Å] is in accordance with those previously reported for $(FeL)_2O$ (1.76–1.82 Å).[31] The combination of the nonlinear bridge and the strong Fe–μ-O bonding produces an intermetallic spacing of 3.5417 Å. The bond lengths of C–N and C–C in the phenanthroline all fall within the range of the literature values,[32] and the two aromatic ring systems in each phen are coplanar within the experimental error.

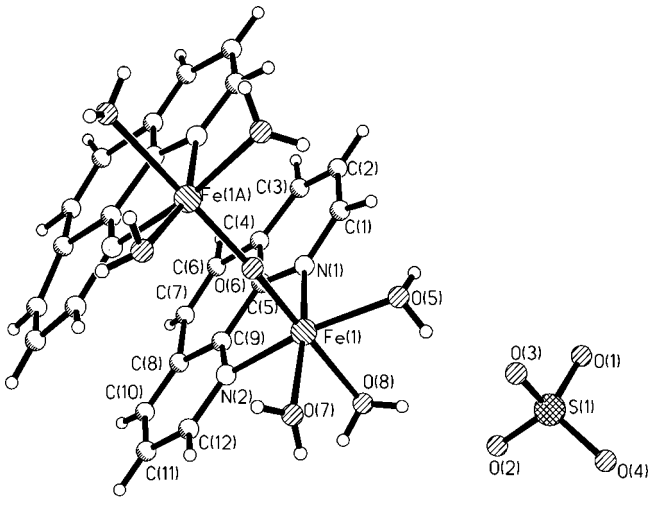

Figure 1. Perspective view of $\{[Fe(phen)(H_2O)_3]_2O\}(SO_4)_2$ showing the atom labeling scheme.

Studies on the Electrochemical Behavior of $\{[Fe(phen)(H_2O)_3]_2O\}^{4+}$

The cyclic voltammetry (CV) of $\{[Fe(phen)(H_2O)_3]_2O\}^{4+}$ in a 0.01 M NaOAc/HOAc solution at a gold electrode was investigated, and the results are shown in Figure 2. It is found that the complex has a cathodic peak (p_1) at +0.325 V and a pair of redox peaks (p_2 and p_2') at +1.011 V and +0.811 V, respectively. From Figure 2b, the formal potential ($E^{0\prime}$) of the redox peaks (p_2 and p_2') was calculated to be +0.911 V, with the formula $E^{0\prime} = (E_{p_2}+E_{p_2'})/2$. This potential is consistent with that reported for the conversion of ferrous complexes to ferric complexes,[33] and suggests that this pair of redox peaks may be attributed to the electro-oxidation and electro-reduction of the mononuclear iron complex. The ratio of the peak height of p_2' to that of p_2 is much smaller than that for the complex $Fe^{III/II}$-(*tris*-phen); this may result from the lack of phen coordinating to the iron atom.[34] The electron transfer number (n) of the irreversible reduction peak p_1 was calculated to be 2 according to the formula $|E_p–E_{p/2}| = 47.7/n\alpha$ (mV, 25 °C) when α is assumed to be 0.5,[35] (E_p and $E_{p/2}$ are the peak potential and the half-peak potential, respectively, α the electron transfer coefficient). This indicates that the two trivalent iron atoms in the title complex have been reduced to a diferrous analog. The peak potential of p_1 (+0.325 V) is almost the same as the reduction potential reported for similar diiron(III) complexes.[36] According to these results, we speculate that the electrode reaction of the title diiron(III) complex may involve an EC–C–EC process, which is described in Scheme 1.

There are similar mechanisms in the literature. Walczak et al. have studied the electrochemical behavior of the oxo-bridged diiron-phen complex $[Fe_2^{III,III}O(phen)_4(H_2O)]^{4+}$ and reached the conclusion that the complex undergoes a 2e reduction to an oxo-bridged diferrous-phen complex $[Fe_2^{II,II}O(phen)_4(H_2O)_2]^{2+}$, which is unstable and quickly decomposes by a fast chemical reaction to form its mononuclear ferrous complex.[36] The electro-redox processes of the $Fe^{II/III}$ complex result in a pair of redox peaks. Chen[37] and other authors[38–39] have also studied the electrochemical behavior of oxo-bridged diiron complexes under different conditions and have obtained similar results. Namely, the electrochemical processes of these species appear as an irreversible reduction peak, corresponding to the re-

 © 2006 Wiley-VCH Verlag GmbH & Co. KGaA, Weinheim

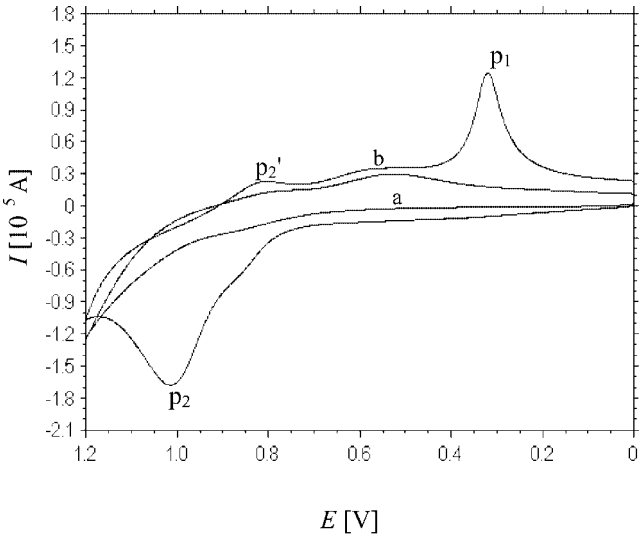

Figure 2. Cyclic voltammograms of 0.01 M NaOAc/HOAc solution, pH 6.8, without (a) and with 4.00×10^{-4} M $\{[Fe(phen)(H_2O)_3]_2O\}^{4+}$ (b). Rest time: 2 s. Scan rate: 100 mV/s.

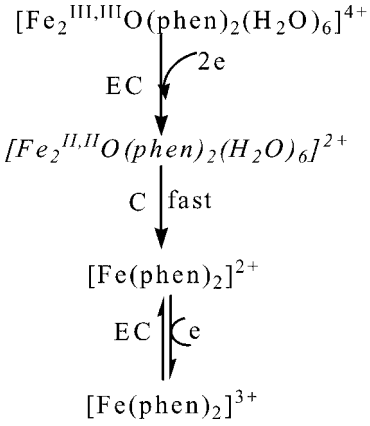

Scheme 1. Electrochemical mechanism of the complex $\{[Fe(phen)(H_2O)_3]_2O\}^{4+}$. The italic font of $[Fe_2^{II,II}O(phen)_2(H_2O)_6]^{2+}$ implies that this intermediate product is unstable.

duction of diiron(III) complex, and a pair of redox peaks with the formal potential ($E^{0\prime}$) at approximately +0.911 V, which is ascribed to the redox of the mononuclear iron(II)/(III) complex. Thus, the electrochemical behavior of the title complex reported here is very similar to those described in the conclusions in the literature.

The influence of the initial potential (E_i) on the cyclic voltammetric behavior of the title complex was studied to further prove the above theory involving the EC–C–EC mechanism of the diiron(III) complex. The results are shown in Figure 3. When the cyclic voltammogram was recorded in the potential range 0.400–1.200 V with an E_i of 0.400 V, there were no longer any electro-redox peaks (Figure 3a), suggesting that no mononuclear iron complex was present in the solution. If E_i was set to +1.000 V, and the potential was scanned in the negative direction towards 0 V and then back to +1.200 V, the reduction peak (p_2') for the mononuclear ferric complex still does not appear; while at +0.325 V, there is an obvious reduction peak (p_1) that corresponds to the reduction of the title diiron(III) complex. There is a well-defined oxidation peak corresponding to the oxidation of the mononuclear divalent iron complex to the trivalent form (Figure 3b). If E_i was set to 0 V, which is more negative than the reduction potential of the title complex, and the cyclic voltammogram ranging from 0 V to +1.200 V was recorded, all the peaks appear (Figure 3c). This experiment demonstrates that the prerequisite for the formation of the mononuclear ferrous complex is the electro-reduction of the title oxo-bridged diiron(III) complex, which is consistent with the proposed EC–C–EC mechanism.

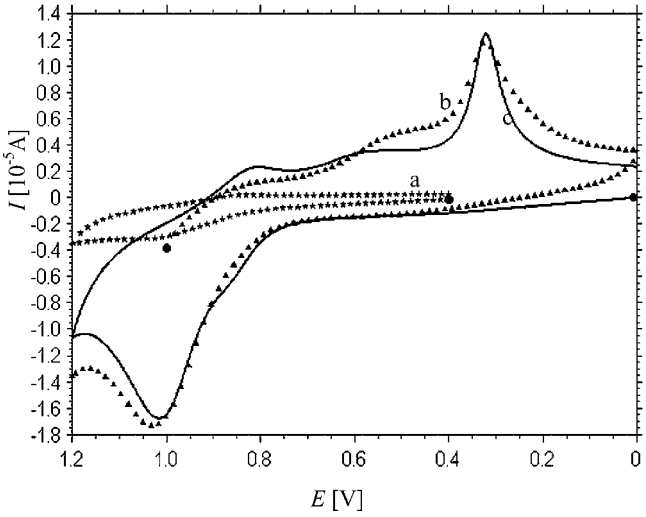

Figure 3. Dependence of the cyclic voltammograms of 4.00×10^{-4} M $\{[Fe(phen)(H_2O)_3]_2O\}^{4+}$ in 0.01 MNaOAc/HOAc solution (pH 6.8) on the initial scan potential (E_i, represented by ●). (a) E_i = 0.400 V, a cyclic scan in the potential range from 0.400 to 1.200 V; (b) E_i = 1.000 V, the scan from 1.000 to 0 V, followed by a positive scan from 0 to +1.200 V; (c) E_i = 0 V, the scan from 0 to +1.200 V, and then scanned reversibly to 0 V. Scan rate: 100 mV/s.

In the following electrochemical studies, only the cathodic peak p_1 and the anodic peak p_2 are considered, as they represent the different species involved in the electrochemical processes and are more sensitive than the cathodic peak p_2'.

Studies on the Interaction of the Iron-Phen Complex with DNA

UVIVis Spectroscopy

As shown in Figure 4a, the complex has a broad absorption band and a sharp peak in the spectral region 200–320 nm, and a weak absorption band in the range 380–520 nm, which is magnified in the inset of Figure 4. From comparison with the spectral data from the paper by Que Jr. et al.[40] and with those from previously studied oxo-diiron(III) complexes,[41] it is known that the lower energy band is assigned to a phenolate-to-Fe^{III} charge-transfer transition, and the higher energy band has been attributed to both phenolate- and oxo-to-Fe^{III} charge-transfer transitions. While, the 300–400 nm region is featureless in Figure 4, the broad and weak absorption peak around 500 nm

 © 2006 Wiley-VCH Verlag GmbH & Co. KGaA, Weinheim

is probably related to a small amount of phen-ligated ferrous complex, as the dinuclear unit is somewhat oxidative under the present conditions. After the addition of dsDNA to the diiron(III) complex solution, it is clearly observed that the absorption peaks in the 200–300 nm region undergo a significant decrease in molecular absorption (the hypochromism effect) and no detectable shift in wavelength (Figure 4b–c).

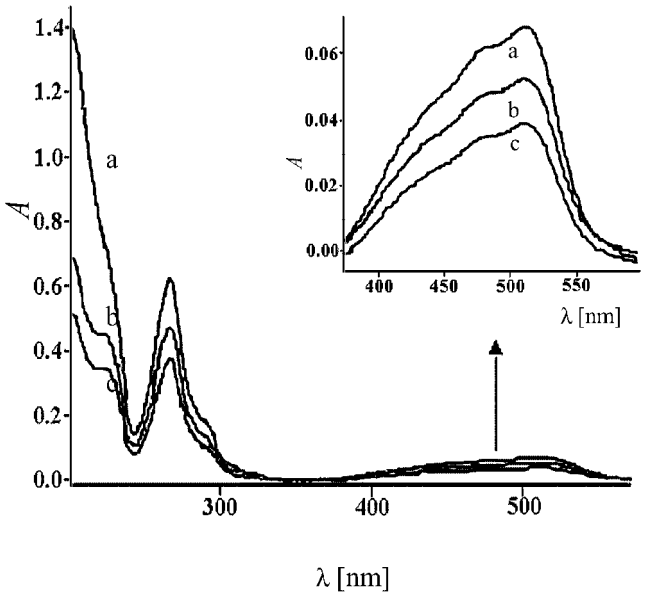

Figure 4. UV/Vis spectra of 4.00×10^{-4} M $\{[Fe(phen)(H_2O)_3]_2O\}^{4+}$ in the absence (a) and the presence of 3.69×10^{-6} M (b) and 7.37×10^{-6} M (c) DNA.

Similarly, the broad absorption band around 500 nm, ascribed to the charge transfer transition of the ferrous complex, decreases gradually and is accompanied by a weak red shift (≈2 nm) from 507.7 nm to 509.6 nm, as shown in the inset in Figure 4. In the case of 1,10-phenanthroline metal complexes, some authors have pointed out that these species interact with dsDNA mainly by the outside-binding mode,[42] while other authors suggest that the binding mode is through intercalation, which involves a stacking interaction of the aromatic chromophores with the base-pairs of the dsDNA duplex.[43] In this paper, according to the rule that when small molecules interact with dsDNA differences in binding mode are reflected by spectral changes,[44] we can speculate that the original diiron(III) complex interacts with dsDNA mainly through external electrostatic binding, while a small amount of the ferrous complex probably binds through intercalation. This rationale is plausible because the size of the ferrous complex is much smaller than that of the diiron(III) complex. This difference in binding mode will be tested by the following electrochemical experiments.

Electrochemical Recognition of dsDNA and ssDNA

Figure 5 shows the cyclic voltammetric behavior of $\{[Fe(phen)(H_2O)_3]_2O\}^{4+}$ after reacting with dsDNA and ssDNA. From Figure 5b, it is observed that the currents of both p_1 and p_2 decrease significantly in the presence of dsDNA, which proves that both the original oxo-bridged diiron complex and its EC–C product can interact with dsDNA. Nonetheless, it is interesting that the potentials of p_1 and p_2 shift in different directions after reacting with dsDNA. Bard et al. have pointed out that the shift direction of the electrochemical potential of a small molecule, after reacting with DNA, is related to its binding mode with DNA. A positive shift of the peak potential indicates an intercalative interaction between the small molecule and DNA, and a negative shift is characteristic of an electrostatic interaction.[45] Therefore, according to this rule, we can conclude that $\{[Fe(phen)(H_2O)_3]_2O\}^{4+}$ may interact with dsDNA through an electrostatic interaction, while its EC–C product interacts by intercalation. It is noticeable that when varying the pH values of the NaOAc/HOAc solution, the current difference of p_2 (ΔI_{p_2}) and p_1 (ΔI_{p_1}) reach maximum values at pH 6.8 and pH 5.5, respectively, after reacting with dsDNA (data not shown). Since pH 6.8 is closer to natural biological conditions, and hence can avoid the denaturing of dsDNA, which occurs at high or low acidity, a NaOAc/HOAc solution at pH 6.8 was chosen as the supporting electrolyte.

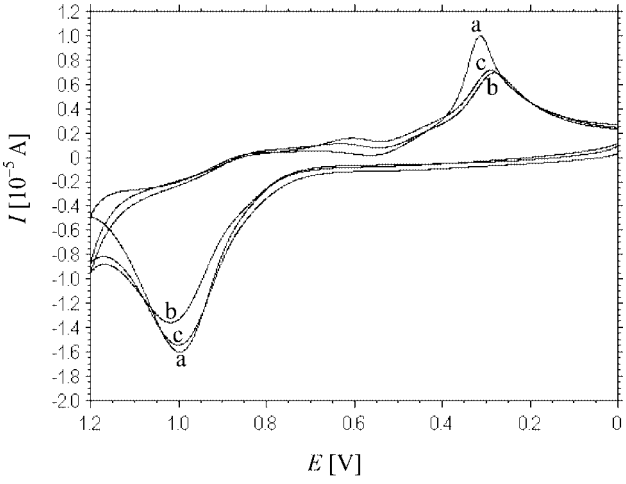

Figure 5. Cyclic voltammograms of 2.00×10^{-4} M $\{[Fe(phen)(H_2O)_3]_2O\}^{4+}$ in 0.01 M NaOAc/HOAc solution at pH 6.8 (a), and after the addition of 2.68×10^{-7} M dsDNA (b) and 2.68×10^{-7} M ssDNA (c). Rest time: 2 s, scan rate: 100 mV/s.

The change in the cyclic voltammetric behavior of $\{[Fe(phen)(H_2O)_3]_2O\}^{4+}$ after reacting with ssDNA confirms the above conclusions. As shown in Figure 5c, both the peak current and the peak potential of p_1 change relative to those in Figure 5b, illustrating that the electrostatic binding between the diiron(III) complex and ssDNA still exists. However, the inconspicuous changes in both the peak current and the peak potential of p_2, relative to those in Figure 5a, indicate the disappearance or weakness of the intercalation of the mononuclear ferrous complex into ssDNA. This can be ascribed to the uncoiling of the double helix structure because of the denaturing of the native DNA. According to the above experiments, we can conclude that the oxo-bridged diiron complex and the mononuclear ferrous complex bind to DNA through different modes. In other words, the diiron(III) complex can recognize

 © 2006 Wiley-VCH Verlag GmbH & Co. KGaA, Weinheim

dsDNA and ssDNA on the basis of the two steps of the electrochemical process on a gold electrode. To further confirm the above conclusions on the binding modes of $\{[Fe(phen)(H_2O)_3]_2O\}^{4+}$ and its mononuclear product to DNA, the influence of ionic strength on their interactions was investigated, and the results are reported in the following section.

Figure 6 shows the effect of the ionic strength (μ) on the peak potential of p_2. The change in the ionic strength was controlled by the addition of different concentrations of KCl. In the absence of dsDNA, the shift in the anodic peak potential ($\Delta E_{p_{2,a}}$) induced by the addition of KCl is obtained by the relation $\Delta E_{p_{2,a}} = E_{p_{2,a}} - E_{p_{2,a,\mu=20}}$, where $E_{p_{2,a}}$ and $E_{p_{2,a,\mu=20}}$ represent the peak potentials of p_2 in the presence and absence of KCl in solution, respectively.

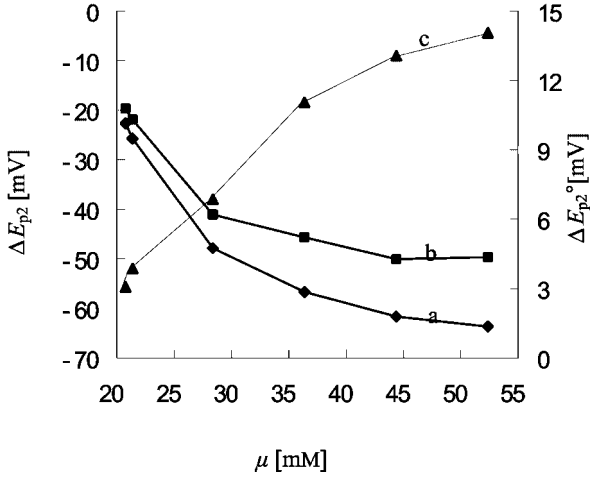

Figure 6. Effect of ionic strength (μ) on the shift in the anodic peak potential (ΔE_{p_2}) of the EC–C product of 4.00×10^{-4} M $\{[Fe(phen)(H_2O)_3]_2O\}^{4+}$, in the absence (a) and the presence of 7.40×10^{-6} M dsDNA (b). Curve (c) is the plot of $\Delta E_{p_2}°$ versus μ, where $\Delta E_{p_2}° = \Delta E_{p_{2,b}} - \Delta E_{p_{2,a}}$.

The subscript "a" and "$\mu = 20$" in the formula indicate that DNA is absent from the solution and that the original ionic strength calculated for the 0.01 M NaOAc/HOAc electrolyte is 20 mM, respectively. Analogously, when DNA is present in solution, the shift in E_{p_2} caused by the ionic strength is denoted as $\Delta E_{p_{2,b}}$, and its value is obtained by the formula $\Delta E_{p_{2,b}} = E_{p_{2,b}} - E_{p_{2,b,\mu=20}}$. Curve a and b in Figure 6 are the plots of $\Delta E_{p_{2,a}}$ versus μ and $\Delta E_{p_{2,b}}$ versus μ, respectively. From the two curves, it is found that both $\Delta E_{p_{2,a}}$ and $\Delta E_{p_{2,b}}$ are negative on the time scale of CV measurements. Furthermore, the values of $\Delta E_{p_{2,a}}$ and $\Delta E_{p_{2,b}}$ decrease gradually with an increase in μ, which suggests that, whether DNA exists in solution or not, the oxidation potential of the phen-ligated ferrous complex shifts to more negative values after the addition of KCl. Nonetheless, the values of $\Delta E_{p_2}°$ reveal the real effect of the ionic strength on the binding of $Fe(phen)_2^{2+}$ to dsDNA, and are positive on the time scale of the CV measurements and increase with an increase in μ, as shown in Figure 6c. According to the literature,[46] the positive shift in $\Delta E_{p_2}°$ induced by the increase in the ionic strength demonstrates the intercalative binding mode of the mononuclear iron complex to dsDNA. This result is also consistent with the hypothesis drawn from Figure 5 with regard to the binding mode of the EC–C product to dsDNA.

However, the change in the reduction peak potential of $\{[Fe(phen)(H_2O)_3]_2O\}^{4+}$ (E_{p_1}) with an increase in the ionic strength is much more complicated. As shown in Figure 7a, the difference ($\Delta E_{p_{1,a}}$) between E_{p_1} at $\mu > 20$ and that at $\mu = 20$ in the absence of dsDNA is negative and decreases with an increase in the ionic strength. This indicates that the reduction peak potential of $\{[Fe(phen)(H_2O)_3]_2O\}^{4+}$ also shifts negatively with an increase in the ionic strength in the absence of dsDNA. After binding to dsDNA, the plot of $\Delta E_{p_{1,b}}$ versus μ has a turning point at $\mu = 24$ mM with an increase of the ionic strength, as shown in Figure 7b. For $\mu < 24$ mM, $\Delta E_{p_{1,b}}$ decreases with an increase in μ and then increases for $\mu > 24$ mM. The plot of $\Delta E_{p_1}°$ ($\Delta E_{p_1}° = \Delta E_{p_{1,b}} - \Delta E_{p_{1,a}}$) versus μ shows the real effect of μ on the binding of $\{[Fe(phen)(H_2O)_3]_2O\}^{4+}$ to dsDNA and is presented in Figure 7c. The dashed line divides the plot into two regions corresponding to $\Delta E_{p_1}° < 0$ and $\Delta E_{p_1}° > 0$. This also demonstrates the change in the nature of the interaction between dsDNA and $\{[Fe(phen)(H_2O)_3]_2O\}^{4+}$ from electrostatic to an intercalative mode with an increase in the ionic strength. At $\Delta E_{p_1}° = 0$, the electrostatic interaction is equal to the intercalative interaction in strength, and the corresponding value for the ionic strength ($\mu = 29$ mM) is called the critical-ionic strength (CIS).[46]

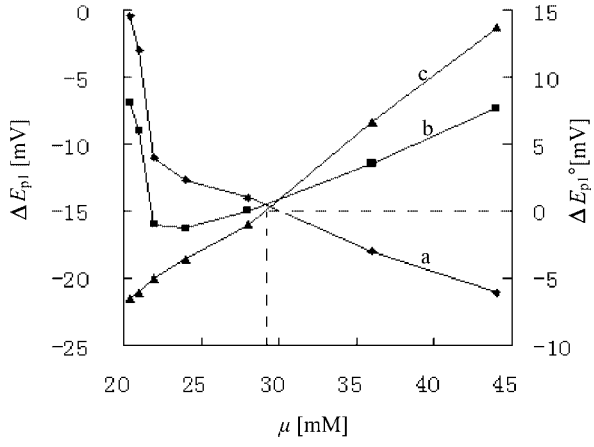

Figure 7. Effect of the ionic strength (μ) on the shift in the reduction peak potential of $\{[Fe(phen)(H_2O)_3]_2O\}^{4+}$. The conditions are the same as those in Figure 6.

From electrostatic considerations, $\Delta E_{p_1}°$ should vary linearly with $\mu^{1/2}$ according to Debye–Hückel theory.[47] Figure 8 illustrates the dependence of $\Delta E_{p_1}°$ on $\mu^{1/2}$. It is observed that the plot is linear for μ up to 28 mM, with an intercept of –38 mV and a slope of 7 mV/mmol$^{1/2}$, which suggests that electrostatic interactions play a dominant role in this ionic strength range. For values of the ionic strength above 28 mM, $\Delta E_{p_1}°$ deviates from a straight line. These observations also prove the results mentioned above with regard to the change in binding mode of {[Fe(phen)-

 © 2006 Wiley-VCH Verlag GmbH & Co. KGaA, Weinheim

$(H_2O)_3]_2O\}^{4+}$ to dsDNA, that is, from electrostatic binding to intercalative binding with an increase in the ionic strength. In addition, from the value of the intercept of –38 mV, a limiting ratio (K_O'/K_R') from the binding constants for the oxidized (K_O') and reduced (K_R') forms ($\{[Fe(phen)(H_2O)_3]_2O\}^{4+}$ and $\{[Fe(phen)(H_2O)_3]_2O\}^{2+}$, respectively) can be estimated. A value of 19 is found for the ratio with the equations $\Delta E^{0\prime} = \Delta E_1^{0\prime} + B\mu^{1/2}$ (for $C_{KCl} << 1$ M)[46] and $\Delta E_1^{0\prime} = (-RT/nF)\ln(K_O'/K_R')$,[45–48] where $\Delta E_1^{0\prime}$ is the limiting difference in the formal potential at $\mu = 0$; B is a constant which depends on the valences of the ions, the dielectric characteristics of the environment surrounding the ions , temperature, and the density of the solvent. This result suggests that the electrostatic interaction between the diiron(III) complex and DNA is significantly more dominant than the intercalative interaction.[45–46]

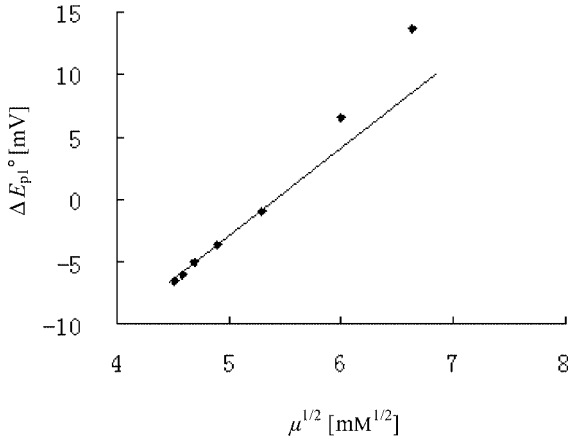

Figure 8. Dependence of ΔE_{p_1}° on $\mu^{1/2}$. The conditions are the same as those in Figure 6.

The effect of the ionic strength on the difference in peak currents before and after the addition of dsDNA was also investigated. It was found that both the cathodic and anodic peak current difference (ΔI_{p_1} and ΔI_{p_2}) decrease with an increase in the ionic strength, as shown in Figure 9a and Figure 9b, respectively. This suggests that the extent of the binding of both the diiron(III) complex and its EC–C product to dsDNA becomes weaker at high ionic strength.

This can be explained by the fact that the excess positively charged K^+ ion binds to negatively charged dsDNA phosphatediester backbone, which results in an inhibition in the binding of the cationic complex to dsDNA.[49]

The dependenc of the cyclic voltammetric behavior of the dinuclear iron(III) complex in the absence and presence of dsDNA on the scan rate (v) are shown in Figure 10(A) and Figure 10(B), respectively. It is found that both I_{p_1} and I_{p_2} vary linearly with the square root of the scan rate ($v^{1/2}$) both in the absence and presence of dsDNA, as shown in the insets of Figure 10(A) and Figure 10(B). This is as expected for a diffusion-controlled process.[50]

Furthermore, the slopes of both plots (I_{p_1} versus $v^{1/2}$ and I_{p_2} versus $v^{1/2}$) decrease after the addition of dsDNA, which indicates a reduction in the apparent diffusion coefficient of the complex in the presence of dsDNA.We can therefore

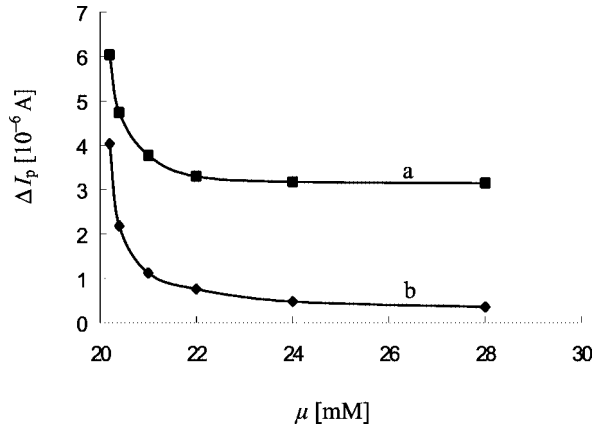

Figure 9. Influence of ionic strength (μ) on ΔI_{p_1} (a) and ΔI_{p_2} (b). The conditions are the same as those in Figure 6.

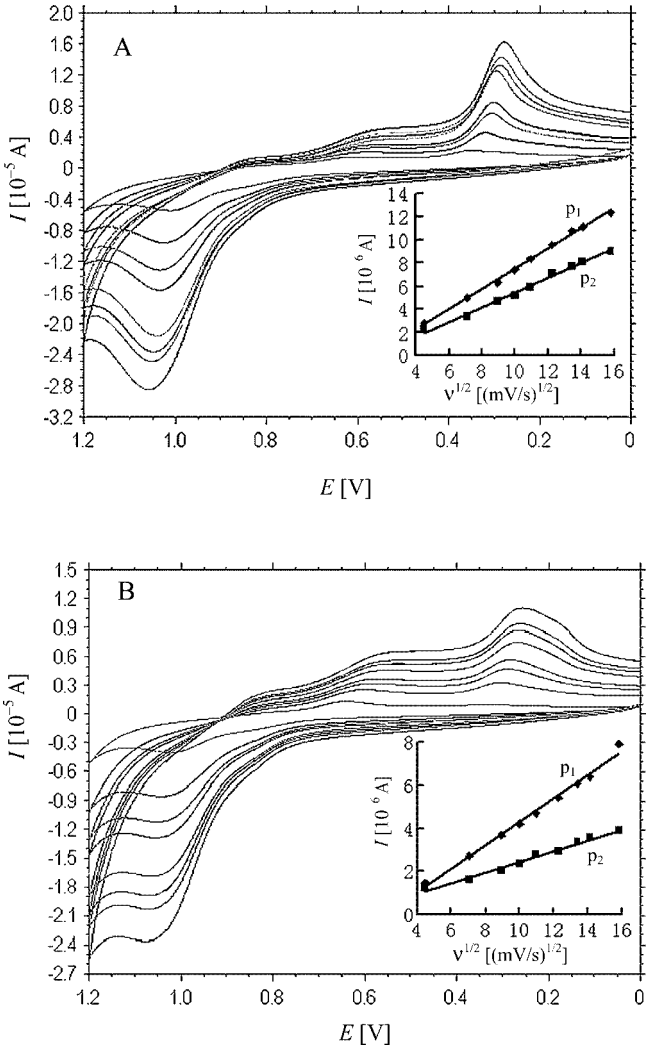

Figure 10. Dependenc of cyclic voltammetric behavior of 4.00×10^{-4} M $\{[Fe(phen)(H_2O)_3]_2O\}^{4+}$ on the scan rate (v), in the absence (A) and the presence (B) of 7.37×10^{-6} M dsDNA. Inset: plots of the peak current of p_1 and p_2 versus the square root of the scan rate ($v^{1/2}$).

 © 2006 Wiley-VCH Verlag GmbH & Co. KGaA, Weinheim

interpret the change in current upon dsDNA addition in terms of the diffusion of an equilibrium mixture of free and dsDNA-bound complex to the electrode surface.[46]

The relationship of both ΔI_{p_1} and ΔI_{p_2} to the concentration of dsDNA (C_{DNA}) was also studied. From Figure 11a, it can be seen that the relationship between ΔI_{p_1} and C_{DNA} is linear in two C_{DNA} ranges corresponding to 9.36×10^{-7}–9.36×10^{-6} M and 9.36×10^{-6}–7.49×10^{-5} M, with correlation coefficients of 0.985 and 0.998, respectively. ΔI_{p_2} becomes constant when the C_{DNA} is larger than 1.87×10^{-5} M (Figure 11b), which demonstrates that the intercalation between the ferrous complex and dsDNA is saturated when the concentration of dsDNA is over 1.87×10^{-5} M.

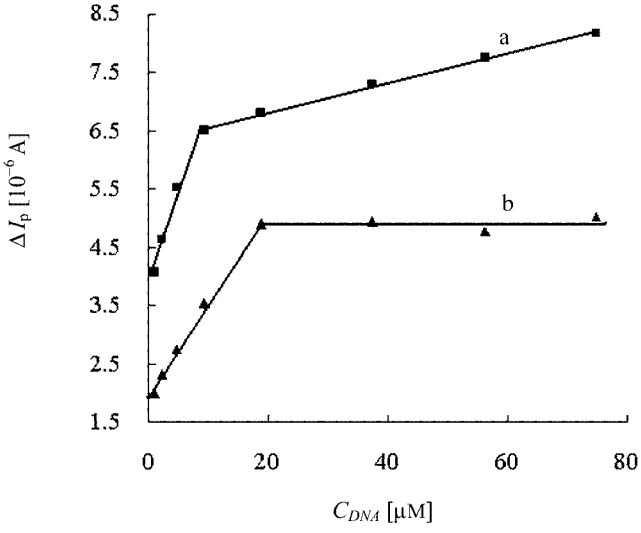

Figure 11. Plots of ΔI_{p_1} (a) and ΔI_{p_2} (b) versus the concentration of dsDNA (C_{DNA}).

Conclusions

In summary, a new dinuclear iron(III) complex $\{[Fe(phen)(H_2O)_3]_2O\}(SO_4)_2$ was synthesized and characterized by X-ray crystallography. The electrochemical behavior of the diiron(III) complex indicated an EC–C–EC mechanism at the gold electrode, and the binding mode of the diiron(III) complex and its final mononuclear product to dsDNA was studied in detail. The results indicate that $\{[Fe(phen)(H_2O)_3]_2O\}(SO_4)_2$ interacts with dsDNA mainly through electrostatic binding, while the mononuclear EC–C product interacts mainly by intercalation. On the basis of its electrochemical behavior, the complex may be an effective recognition probe for dsDNA and ssDNA.

Experimental Section

Chemicals and Measurements: Native double-stranded fish sperm DNA (dsDNA) from Beijing Baitai Biochemistry Technology Company (China) was used as received. The ratio of the absorbance at 260 and 280 nm (A_{260}/A_{280}) was checked to be 1.89, which indicates that the DNA was sufficiently free from protein.[51] The concentration of dsDNA (per nucleotide phosphate) was determined spectrophotometrically using the known molar-extinction coefficient value of 6600 $M^{-1}cm^{-1}$.[52] Denatured single-stranded DNA (ssDNA) was produced by heating a dsDNA solution in a water bath at 100 °C for 5–6 min, followed by rapid cooling in an ice bath.[46] The other chemical reagents used in the synthesis of the title complex were all of analytical reagent grade, purchased commercially, and used without further purification. The electrochemical and spectroscopic assays were all carried out in 0.01 M NaOAc/HOAc medium. Double-distilled water was used for preparing all the solutions. Elemental analyses were measured with a Perkin–Elmer 1400C analyzer. Voltammetry was performed with a CHI 832 electrochemical analysis system (CHI Instrument, China). A three-electrode system was used which consisted of a gold electrode (Φ = 3 mm) as the working electrode, a saturated calomel electrode (SCE) as the reference electrode, and a platinum wire as the auxiliary electrode. All the electrochemical measurements were carried out in a 10 mL electrolytic cell. UV/Vis absorption spectra were recorded on a Cary 50 probe spectrophotometer (Varian, Australia).

Preparation and Crystallographic Study of $\{[Fe(phen)(H_2O)_3]_2O\}(SO_4)_2$: 1,10-phenanthroline (0.35 g, 2.0 mmol) was dissolved in ethanol (15 mL), and a 10 mL solution of iron(III) chloride hexahydrate (0.28 g, 1.0 mmol) was then added while stirring. The mixture was adjusted to a pH of 1.0 with a dilute sulfuric acid solution and sealed in a 50 mL stainless-steel reactor with Teflon liner. The reactor was heated at 100 °C for 72 h, which resulted in the formation of red crystals. C, H and N contents were determined by elemental analysis. $C_{24}H_{28}Fe_2N_4O_{15}S_2$ (788.32): calcd. C 36.53, H 3.55, N 7.10; found C 36.16, H 3.30, N 6.82.

The X-ray diffraction data for the crystal-structure determination was collected using graphite-monochromated Mo-K_α radiation (λ = 0.71073 Å) and ω-scans with θ limits $2.04° < \theta < 27.52°$. An empirical absorption correction was carried out with the SADABS program.[53] The structure of $\{[Fe(phen)(H_2O)_3]_2O\}(SO_4)_2$ was

Table 1. Crystal data and structure refinement for $\{[Fe(phen)(H_2O)_3]_2O\}(SO_4)_2$.

Empirical formula	$C_{24}H_{28}Fe_2N_4O_{15}S_2$
Formula weight	788.32
Temperature [K]	293(2)
Wavelength [Å]	0.71073
Crystal system, space group	Orthorhombic, $P2_12_12$
Unit cell dimensions	
a [Å]	17.650(4)
b [Å]	8.5133(17)
c [Å]	9.971(2)
Volume [Å^3]	1498.2(5)
Z, Calculated density [Mg/m^3]	4, 1.748
Absorption coefficient [mm^{-1}]	1.189
F(000)	808
Crystal size [mm]	$0.20\times0.20\times0.30$
θ range for data collection [°]	2.04–27.52
Limiting indices	$-22 \le h \le 22$
	$-11 \le k \le 11$
	$0 \le l \le 12$
Reflections collected/unique	5376/3101[$R_{(int)}$ = 0.0618]
Completeness to θ = 27.53 [%]	93.7
Refinement method	Full-matrix least-squares on F^2
Data/restraints/parameters	3101/0/214
Goodness-of-fit on F^2	1.010
Final R indices[$I > 2\sigma(I)$]	R_1 = 0.0558, wR_2 = 0.1338
R indices (all data)	R_1 = 0.0762, wR_2 = 0.1417
Extinction coefficient	0.0081(18)
Largest diff. peak and hole [e Å^{-3}]	0.551 and –0.448

 © 2006 Wiley-VCH Verlag GmbH & Co. KGaA, Weinheim

solved by direct methods and refined by least-squares on $F_{obsd.}^2$ by using the SHELXTL software package.[54] All non-H atoms were anisotropically refined. The hydrogen atoms were located by difference synthesis and refined isotropically. The final conventional R indices were $R(F) = 0.0601$ and $wR(F^2) = 0.1496$ for 2391 reflections $I > 2\sigma(I)$ with weighting scheme, $w = 1/[\sigma^2(F_o^2) + (0.0905P)^2]$, where $P = (F_o^2 + 2F_c^2)/3$. The molecular graphics were plotted using SHELXTL. Atomic scattering factors and anomalous dispersion corrections were taken from the *International Tables for X-ray Crystallography*.[55] A summary of the key crystallographic information is given in Table 1. CCDC-227065 contains the supplementary crystallographic data for this paper. These data can be obtained free of charge from The Cambridge Crystallographic Data Centre via www.ccdc.cam.ac.uk/data_request/cif.

Acknowledgments

This work is supported by the National Natural Science Foundation of China (Grant No. 20375020, No. 20405008) and Natural Science Foundation of Qingdao City (Grant No. 04-2-JZP-8, No. 04-2-JZ-114).

[1] R. T. Espejo, J. Lebowitz, *Anal. Biochem.* **1976**, *72*, 95–103.
[2] M. Mariappan, B. G. Maiya, *Eur. J. Inorg. Chem.* **2005**, 2164–2173.
[3] J. K. Barton, A. L. Raphael, *Proc. Natl. Acad. Sci. USA* **1985**, *82*, 6460–6464.
[4] M. Kobayashi, T. Kusakawa, M. Saito, K. Sakiko, M. Oomura, S. Iwabuchi, Y. Morita, Q. Hasan, T. Eiichi, *Electrochem. Commun.* **2004**, *6*, 337–343.
[5] H. J. Karlsson, P. Lincoln, G. Westman, *Bioorg. Med. Chem.* **2003**, *11*, 1035–1040.
[6] J. P. Zheng, Z. Li, A. G. Wu, H. L. Zhou, H. Y. Bai, Y. H. Song, *Biochem. Biophys. Res. Commun.* **2002**, *299*, 910–915.
[7] G. V. Kalayda, S. Komeda, K. Ikeda, T. Sato, M. Chikuma, J. Reedijk, *Eur. J. Inorg. Chem.* **2003**, 4347–4355.
[8] J. Y. Douillard, D. Cunningham, A. D. Roth, J. R. Germa, R. D. James, P. Karasek, P. Jandik, J. Iveson, J. Carmichael, *Proc. Am. Soc., Clin. Oncol.* **1999**, *18*, 899–905.
[9] F. P. Intini, A. B. V. C. Francia, C. P. M. F. Sivo, G. Natile, D. G. P. D. Rinaldis, M. Coluccia, *J. Biol. Inorg. Chem.* **2004**, *9*, 768–780.
[10] P. G. Sammes, G. Yohioglu, *Chem. Soc. Rev.* **1994**, *23*, 327–334.
[11] E. J. C. Olson, D. Hu, A. Hormann, A. M. Jonkman, M. R. Arkin, E. D. A. Stemp, J. K. Barton, B. F. Barbara, *J. Am. Chem. Soc.* **1997**, *119*, 11458–11467.
[12] C. S. Chow, F. M. Bogdan, *Chem. Rev.* **1997**, *97*, 1489–1514.
[13] K. Gisselfalt, P. Lincoln, B. Norden, M. Jonsson, *J. Phys. Chem. B* **2000**, *104*, 3651–3659.
[14] S. Arounaguiri, B. G. Maiya, *Inorg. Chem.* **1996**, *35*, 4267–4267.
[15] M. N. Yoshioka, H. Inoue, *J. Inorg. Biochem.* **1999**, *77*, 239–247.
[16] T. Hard, B. Norden, *Biopolymers* **1986**, *25*, 1209–1228.
[17] T. Kobayashi, S. Nishino, H. Masud, H. Einag, Y. Nishid, *Inorg. Chem. Commun.* **2000**, *3*, 608–610.
[18] A. Silvestri, G. Barone, G. Ruisi, M. T. L. Giudice, S. Tumminello, *J. Inorg. Biochem.* **2004**, *98*, 589–594.
[19] A. Trotta, A. B. Paulsen, A. Silvestri, G. Ruisi, M. A. Girasolo, R. Barbieri, *J. Inorg. Biochem.* **2002**, *88*, 14–18.
[20] A. Silvestri, G. Ruisi, M. A. Girasolo, *J. Inorg. Biochem.* **2002**, *92*, 171–176.
[21] C. L. Liu, M. Wang, T. L. Zhang, H. Z. Sun, *Coordin. Chem. Rev.* **2004**, *248*, 147–168.
[22] L. M. T. Schnaith, R. S. Hanson, L. Que Jr, *Proc. Natl. Acad. Sci. USA* **1994**, *91*, 569–573.
[23] G. Roelfes, M. E. Branum, L. Wang, L. Que Jr, B. L. Feringa, *J. Am. Chem. Soc.* **2000**, *122*, 11517–11518.
[24] C. Liu, S. Yu, D. Li, Z. Liao, X. Sun, H. Xu, *Inorg. Chem.* **2002**, *41*, 913–922.
[25] J. K. Sessler, J. W. Sibert, A. K. Burrell, V. Lynch, J. T. Markert, C. L. Wooten, *Inorg. Chem.* **1993**, *32*, 4277–4283.
[26] P. G. Romero, G. C. DeFotis, G. B. Jameson, *J. Am. Chem. Soc.* **1986**, *108*, 851–853.
[27] S. Menage, J. B. Galey, G. Hussler, M. Seite, M. Fontecave, *Angew. Chem. Int. Ed. Engl.* **1996**, *35*, 2353–2355.
[28] L. Que Jr, A. E. True, *Prog. Inorg. Chem.* **1990**, *38*, 97–103.
[29] A. L. Feig, S. J. Lippard, *Chem. Rev.* **1994**, *94*, 759–805.
[30] D. F. Xiang, X. S. Tan, S. W. Zhang, Y. Han, K. B. Yu, W. X. Tang, *Polyhedron* **1998**, *17*, 2095–2100.
[31] K. S. Murrays, *Coord. Chem. Rev.* **1974**, *12*, 1–35.
[32] Y. P. Tian, C. Y. Duan, X. X. Xu, X. Z. You, *Acta Crystallogr., Sect. C* **1995**, *51*, 2309–2312.
[33] K. Ogura, H. Urable, T. Yosino, *Electrochim. Acta* **1977**, *22*, 285–287.
[34] Y. L. Zhang, H. X. Shen, C. X. Zhang, A. Ottova, H. T. Tien, *Electrochim. Acta* **2001**, *46*, 1251 –1257.
[35] Z. Galus, *Fundamentals of Electrochemical Analysis*, Chichester, Ellis Horwood. **1976**, p. 237.
[36] M. M. Walczak, N. T. Flynn, *J. Electroanal. Chem.* **1998**, *441*, 43–49.
[37] S. M. Chen, *Inorg. Chim. Acta* **1996**, *249*, 143–150.
[38] M. C. Dunand-Sauthier, A. Deronzier, C. D. Toia, M. Fontecave, K. Gorgy, J. Lepretre, S. Menage, *J. Electroanal. Chem.* **1999**, *469*, 53–62.
[39] M. D. Luque de Castro, M. Valcarcel, F. N. Albahadily, H. A. Mottola, *J. Electroanal. Chem.* **1987**, *219*, 139–151.
[40] S. Ménage, L. Que Jr, *New J. Chem.* **1991**, *15*, 431–438.
[41] E. W. Ainscough, A. M. Brodie, J. E. Plowman, K. L. Brown, A. W. Addison, A. R. Gainsford, *Inorg. Chem.* **1980**, *19*, 3655–3663.
[42] S. Satyanarayana, J. C. Dabrowiak, J. B. Chaires, *Biochemistry* **1993**, *32*, 2573–2584.
[43] A. M. Pyle, J. P. Rehman, R. Meshoyrer, C. V. Kumar, N. J. Turro, J. K. Barton, *J. Am. Chem. Soc.* **1989**, *111*, 3051–3058.
[44] J. K. Barton, A. L. Raphael, *J. Am. Chem. Soc.* **1984**, *106*, 2172–2176.
[45] M. T. Carter, M. Rodriguez, A. J. Bard, *J. Am. Chem. Soc.* **1989**, *111*, 8901–8911.
[46] D. W. Pang, H. D. Abruna, *Anal. Chem.* **1998**, *70*, 3162–3169.
[47] H. S. Harned, B. B. Owen, *The Physical Chemistry of Electrolytic Solution*, Reinhold, New York, **1950**, p. 32.
[48] Y. L. Zhang, H. X. Shen, C. X. Zhang, A. Ottova, H. T. Tien, *Electrochim. Acta* **2001**, *46*, 1251–1257.
[49] P. O. Vardevanyan, A. P. Antonyan, G. A. Manukyan, A. T. Karapetyan, *Exp. Mol. Med.* **2001**, *33*, 205–208.
[50] A. J. Bard, L. R. Faulkner, *Electrochemical Methods: Fundamentals and Applications*, Wiley, New York **1980**.
[51] M. E. Reichman, S. A. Rice, C. A. Thomas, P. Doty, *J. Am. Chem. Soc.* **1954**, *76*, 3047–3053.
[52] C. V. Kumar, E. H. Asuncion, *J. Am. Chem. Soc.* **1993**, *115*, 8547–8553.
[53] G. M. Sheldrick, *SADABS*, University of Göttingen, Germany, **1996**.
[54] G. M Sheldrick, *SHELXTL97, Program for Crystal Structure Refinement*, University of Göttingen, Germany, **1993**.
[55] A. J. Wilson, *International Tables for X-ray Crystallography*, V. C, Kluwer Academic Publishers, Dordrecht, Tables 6.1.1.4 and 4.2.6.8, **1992**, p. 500 and p. 219, respectively.

Received: September 16, 2005
Published Online: March 16, 2006

 © 2006 Wiley-VCH Verlag GmbH & Co. KGaA, Weinheim